Spatially Controlled Supramolecular Polymerization of Peptide Nanotubes by Microfluidics

Alejandro Méndez-Ardoy, Alfonso Bayón-Fernández, Ziyi Yu, Chris Abell, Juan R. Granja, Javier Montenegro

Spatially Controlled Supramolecular Polymerization of Peptide Nanotubes by Microfluidics

Alejandro Méndez-Ardoy,[a] Alfonso Bayón-Fernández,[a] Ziyi Yu,[b] Chris Abell,[b] Juan R. Granja,*[a] Javier Montenegro*[a]

Abstract: The recent advances in the supramolecular polymerization of synthetic building blocks in aqueous conditions has given rise to new artificial and biocompatible functional materials. However, despite the importance of spatially resolved self-assembly for natural and artificial molecular machines, the spatial control of supramolecular polymerization with synthetic monomers has not been experimentally established yet. Here, we describe a microfluidic-regulated tandem process of supramolecular polymerization and droplet encapsulation to control the position of self-assembled microfibrillar bundles of cyclic peptide nanotubes in water droplets. This method allowed the precise preferential localization of the fibres either at the interface or into the core of the droplets. UV absorbance, circular dichroism and fluorescence microscopy indicated that the microfluidic control of the stimuli (changes in pH or ionic strength) can be employed to adjust the packing degree and the spatial position of microfibrillar bundles of cyclic peptide nanotubes. Additionally, this spatially organized supramolecular polymerization of peptide nanotubes was applied in the assembly of highly ordered two-dimensional droplet networks.

Introduction

Recent synthetic materials with applications in nanotechnology and medicine are obtained by the non-covalent assembly of biocompatible building blocks.[1] The current progress with the supramolecular polymerization of artificial monomers in aqueous environment has led to promising functional biomaterials and devices.[1] However, in Nature, precise spatiotemporal control of supramolecular self-assembly is important for the modulation of the conditions and the chemical environment of critical biochemical processes.[2] For example, spatially localized supramolecular polymerization is crucial for the transduction of anisotropic mechanical forces[2],[3] such as in protein contractile rings, which must be assembled in very specific locations to ensure the correct cell membrane contractions.[3],[4] A range of simplified confinement synthetic models have been recently designed to understand these polymerization processes and their distribution between the core or the cortex of these artificial containers.[5a-j] Despite much has been advanced with natural proteins, the confined self-assembly of artificial minimal systems that can be engineered by rational design has been much less explored.[6a-d]

Bottom-up approaches towards synthetic mimics of natural supramolecular systems have recently exploited the encapsulation of artificial peptides[7] in protocell mimics,[8] such as giant vesicles,[9] capsules[10] or water-in-oil droplets.[11] However, despite the importance of the precise position of intracellular supramolecular networks, the control over the spatial adjustment of synthetic fibrillar networks has not been experimentally achieved. The recent application of microfluidics to encapsulate biomolecules (e.g. FtsZ, actin, tubulin) has allowed the *in vitro* generation of useful and simple cellular compartments to study biochemical processes and cellular machinery.[12a-c] Current microfluidic technologies allow the preparation of water droplet microcontainers with precise shape, size, volume, composition and internal concentration.[13] Furthermore, the adjustment of the mixing regimes by microfluidics also allows the precise selection of the self-assembly conditions and pathways in supramolecular assemblies.[14]

Supramolecular microfibres made of bundles of hollow nanotubes can be obtained by one dimensional (1D) hierarchical assembly of the suitable cyclic peptide monomers (CP).[11][15] These dynamic structures can be employed to mimic the physical properties of more complex natural fibrillar networks and function as storage or transport systems.[11],[16a-d] Here, we report on the spatially controlled supramolecular polymerization of cyclic peptide nanotubes by a microfluidic-triggered self-assembly process within aqueous droplets. Spatially regulated fibrillar assembly was achieved by the microfluidic control of the chemical stimuli that triggers the polymerization (i.e. pH or ionic strength). A detailed microscopic and spectroscopic characterization was employed to study the self-assembly process, which was precisely adjusted from the cortex interface to the core of the water droplet. Additionally, the spatially controlled supramolecular polymerization of cyclic peptides nanotubes was applied in the two-dimensional (2D) assembly of droplet networks by fibrillation-assisted packing of individual droplet populations.

[a] Dr. A. Méndez-Ardoy, Mr. A. Bayón-Fernández, Prof. Dr. J. R. Granja, Dr. J. Montenegro
Centro Singular de Investigación en Química Biolóxica e Materiais Moleculares (CIQUS) and Departamento de Química Orgánica, Universidad de Santiago de Compostela
15782 Santiago de Compostela (Spain)
E-mail: javier.montenegro@usc.es, juanr.granja@usc.es

[b] Dr. Z. Yu, Prof. Dr. C. Abell
Department of Chemistry,University of Cambridge, Cambridge CB2 1EW, UK.

Supporting information for this article is given via a link at the end of the document.

Results and Discussion

Cyclic peptide (CP) monomers[16a] were employed as building blocks, as they can be precisely designed to trigger their one-dimensional hierarchical polymerization[17a-c] from the nano[16a] to the meso-scale.[11] The CP depicted in Figure 1A (**CP1**) is positively-charged at acidic pH (pH ~ 4) due to protonation of the lysine and the histidines residues, which prevents **CP1** assembly due to electrostatic repulsions. Attenuation of the repulsive forces by either deprotonation (alkalinization) or by counterion shielding (ionic strength) would favour inter-monomer interactions and yield the corresponding self-assembled cyclic peptide nanotubes (SCPNs).[18] In the tubular architecture assembled from **CP1**, the hydrogen-bonded antiparallel β-sheets are stabilized by the hydrophobic and the π-π interactions of the pyrene units (Figure 1A). However, due to the distance mismatch between β-sheets and π-π stacks, the intercalation of pyrene moieties allows the one-dimensional hierarchical arrangement of the corresponding micron sized tubular bundles (Figure 1A, bottom).[11] As previously reported, the pH control of solutions of **CP1** allowed peptide self-assembly assisted by pyrene stacking as shown by the quenching and the bathochromic shift of the fluorescence emission due to excimer formation.[11, 17b,c]

We hypothesized that ionic strength could also be employed to trigger the self-assembly of **CP1** by shielding electrostatic repulsions by counterion scavenging. Typically, electrostatic repulsions decrease by decreasing Debyes double layer thickness, which is inversely proportional to the ionic strength.[19] Therefore, addition of electrolytes should allow the self-assembly of protonated peptide nanotubes.[20a,b] These two different trigger signals (pH and ionic strength) would thus lead to different tubular networks with potential different interactions with the environments of the water droplet (i.e. interface or aqueous inner volume). To test this hypothesis, we first studied the self-assembly of protonated **CP1** in the bulk aqueous buffer by adding a variety of different electrolytes such as $CaCl_2$, NaCl or Na_2SO_4 (see Section S2 in Supporting Information). The corresponding increase of the Cotton effect, assigned to the π-π* transition of the pyrene moiety, confirmed that self-assembly of **CP1** could be triggered by ionic strength modulation (Figure S1A). As expected, this process was more efficient for multivalent anions (SO_4^{2-} *vs* Cl^-) than multivalent cations (Ca^{2+} *vs* Na^+). The fluorescence quenching of the pyrene emission was also observed, as it could be anticipated for the ionic shielding of the cationic charge of the peptide monomers (Figure S1B). Fluorescence microscopy confirmed that ionic strength triggered the fibrillar assembly of **CP1**, which was dependent on the concentration and the chemical nature of the added counterions (Figure S2). The corresponding one-dimensional hierarchical bundles of peptide nanotubes were also confirmed by fluorescence and STEM electron microscopy (Figure S3).

After confirming the hierarchical and efficient self-assembly of cyclic peptides by ionic strength modulation, we hypothesized that the microfluidic-controlled tandem encapsulation and self-assembly of cyclic peptides using different trigger signals (i.e. pH or ionic strength) could be applicable to adjust the packing degree, the chemical nature and the spatial positioning of the resulting supramolecular peptide fibres. The microfluidic device shown in Figure 1B was employed to control the tandem assembly and droplet confinement of **CP1** in the presence or absence of different assembly triggers. We initiated peptide nanotube assembly in junction *J*1 by merging the streams of I_{CP1}, containing a diluted aqueous **CP1** solution (1 mM) and I_T, containing the assembly-triggering solution (i.e., base or highly concentrated saline solutions, Section S3).[21] Droplet encapsulation was immediately achieved in junction *J*2 by flow focusing the aqueous stream with an oil stream composed of HFE 7500 3M Novec and 0.5% v/v Pico-Surf™ as surfactant (I_{oil}).[22] This set up was employed to adjust the flow rates at (I_T) and the different stimuli for the spatially controlled distribution of the nanotubes within the aqueous droplets.

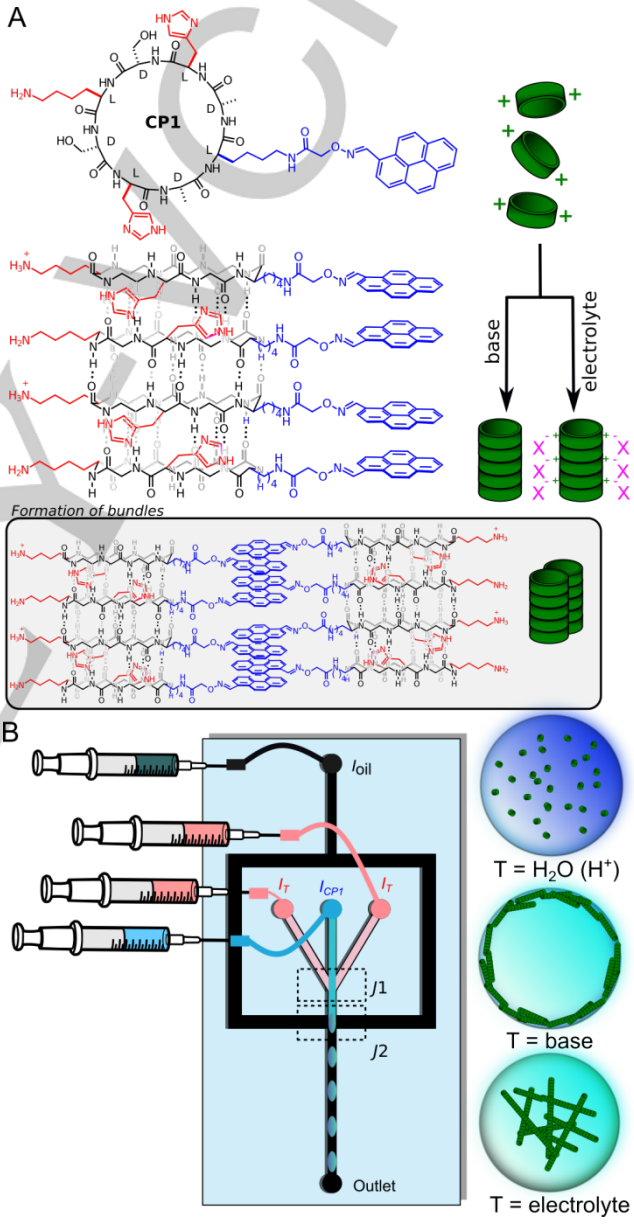

Figure 1. Spatially controlled supramolecular fibrillation. A) Structure and model of pH triggered self-assembly of cyclic peptide **CP1**.[11] Basic amino acids are drawn in red. Pyrene moiety in blue. B) Microfluidic device for the *in situ* fibrillation. Channels dimensions: 35 × 50 μm. **CP1** in aqueous conditions (1 mM, milliQ water, pH 3-4) was injected in inlet I_{CP1} (blue) at flow rates of 200-150 μL/h and assembled upon mixing with inlets I_T containing water, base (NaOH 3.5 mM) or an electrolyte (e.g. $CaCl_2$ 1 M) in junction *J*1 (pink) at flow rates of 100 μL/h. The aqueous stream converges with the oil phase (HFE 7500 3M Novec with 0.5% v/v Pico-Surf™ as surfactant, black) by I_{oil} inlet in *J*2 for droplet generation at flow rates of 500 μL/h. Droplets are collected in *outlet*.

Initial experiments were performed by flowing pure water in the assembly inlets (I_T), which merged in $J1$ with acidic (pH ~ 4) aqueous solution of **CP1** (I_{CP1}) and were encapsulated in droplets ($J2$). Fluorescence microscopy analysis of these droplets showed the typical blue fluorescence emission that belongs to dispersed CPs and monomeric pyrene (Figure 2A,B). As expected, the droplet fluorescence profile and the corresponding confocal planes showed that the pyrene emission was equally distributed along the droplet interior (Figure 2C and Figure 2D). However, when an alkaline solution (NaOH 3.5 mM) was injected in I_T, a red-shifted green fluorescent halo was observed in the droplet periphery (Figure 2E-H). The corresponding micrographs indicated a preferential adsorption of the supramolecular peptide nanotubes and microfibres at the perimeter of the water-droplet interface (Figure 2G-H) in capsule-like structures.[23a,b] Similar results were observed in fibrillation experiments using HEPES buffer (50 mM, pH = 8) as to precisely control the pH increase (see Figure S5). Microfluidic fibrillation experiments by direct base picoinjection ($NaOH_{aq}$), in preformed droplets loaded with homogeneously dispersed **CP1** (pH ~ 4), again showed the assembly of a fluorescent droplet cortex, which was reminiscent of reconstituted actin[5d] or DNA[24] cortical shells (Section S5, Figure S7, Video S1). These picoinjection experiments unambiguously confirmed that the spatial control of the supramolecular polymerization was caused by the modulation of the chemical signal trigger. In contrast to the pH signal, when a solution of high ionic strength ($CaCl_2$, 1 M) was employed to trigger peptide assembly, the resulting fibrillar networks were concentrated at the droplet core from where they spanned the inner volume of the droplets (Figure 2I-L). As shown in the corresponding fluorescent profile, a much lower absorption at the droplet surface and a maximal fibre concentration at the droplet core could be traced (Figure 2K,L). Confocal planes further supported these observations (Figures S8,9 and Video S2 and S3 for NaOH and $CaCl_2$ respectively)

To rationalize these results, the fluorescence emission, the UV-Vis absorbance and the circular dichroism (CD) were measured and compared in exactly the same conditions to those used in the microscopy fibrillation experiments (Figure 3). The CD indicated that the chirality of the assemblies was similar independently of the chemical trigger (Figure 3A). However, comparison of the fluorescence emission of the CP solutions under acidic, alkaline and high ionic strength conditions showed a stronger fluorescence quenching for the fibrillar assemblies at alkaline pH (Figure 3B).[11] Additionally, normalized fluorescence emission spectra, again indicated a higher excimer signal also for the pH increase, which suggested a stronger packing of the pyrene units[17c], as it would be expected for the assembly of the deprotonated cyclic peptide monomers (Figure 3B).

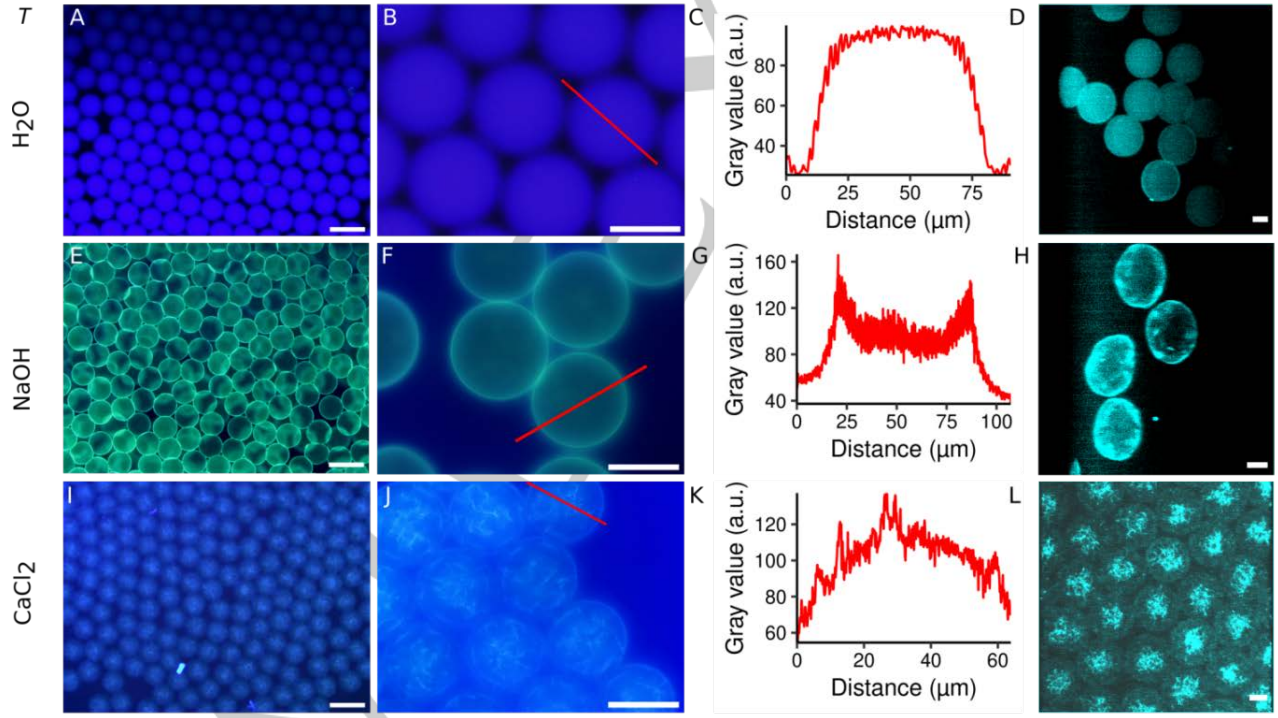

Figure 2. Self-assembly of **CP1** in microfluidic generated droplets (water-in-oil) as function of composition of inlet I_T. Top, middle and bottom rows show the results when I_T is water, NaOH (3.5 mM) and $CaCl_2$ (1 M) respectively. Figures A, E and I are low magnification images with scale bars of 100 μm. Figures B, F and J are high magnification images (scale = 50 μm). C, G and K show profiles extracted from high magnification images (red lines in B, F and J). Figures D, H and L show confocal 3D projections of the droplets (scale = 25 μm). Flow rates were: I_{oil} = 500 μL/h; I_{CP1} = 200-150 μL/h; I_T = 100 μL/h.

To further study the assembly process we employed Thioflavin T (ThT), a fluorescent probe that enhances its fluorescence emission in its planar state when trapped within β-sheets.[25] In these experiments, the self-assembly of **CP1** would bring into close contact the thioflavin probe and the pyrene of the peptide, which should give rise to fluorescence resonance energy transfer (FRET) between the pyrene donor and the ThT exogenous acceptor.[11] As shown in Figure 3C, the ThT emission (FRET effect) was higher for peptide assembled upon alkalinization, which indicated a more efficient and compact nanotube packing of the peptides assembled under basic conditions (Figure 3C). UV-vis spectra also showed a higher decrease in the extinction coefficient of the pyrene in basic conditions, which was again indicative of a stronger pyrene association in the resulting more hydrophobic nanotubes (Figure 3D). These results were consistent with a better supramolecular packing for the more hydrophobic deprotonated fibres obtained by alkalinization, which would have a higher affinity for the droplet oil-water interface. In contrast, fibres assembled under high ionic strength were found to be less packed and to allow higher electrostatic interactions between nanotubes. Therefore, these more hydrophilic tubular bundles have a lower affinity for the droplet interface and concentrate at the droplet core. These series of experiments confirmed that the assembly pathway can lead to different supramolecular polymers with particular affinities for different environments in a single water droplet.

The experimental confirmation of the different assembly pathway and chemical nature of microfluidic-triggered fibrillar networks, prompted us to explore the potential spatial positioning of supramolecular polymers by tuning the flow rate of the corresponding trigger. In this case, modulation of the flow of electrolyte (I_T) would control the molar ratio between the anions and the cationic peptide monomers and thus allow a different degree of ionic shielding of the resulting supramolecular fibres.

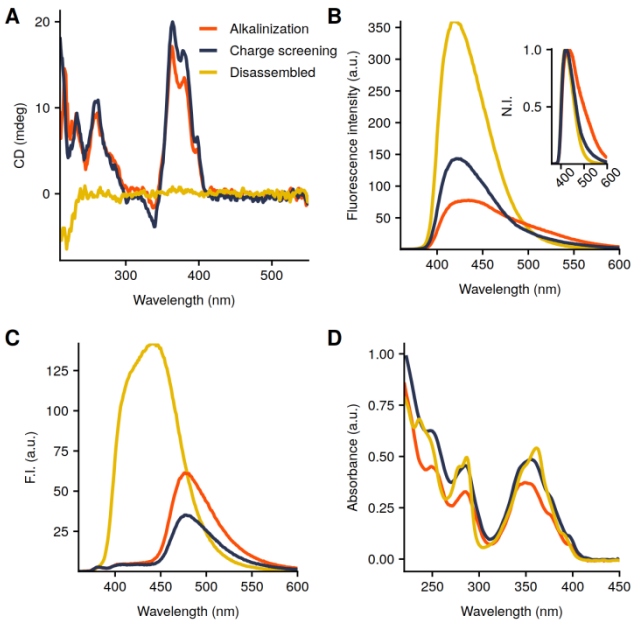

Figure 3. Spectroscopic characterization of **CP1** self-assembly. In all cases conditions by line colours: acidic (HCl pH ~ 4) in yellow, HEPES (50 mM, pH 8) in orange and $CaCl_2$ (500 mM) in blue. A) Circular dichroism of **CP1** (200 μM); B) Pyrene fluorescence emission. (λ_{ex} = 340 nm). *Condition*: pH (80% quenching) and ionic strength (60 % quenching). C) FRET between pyrene and ThT fluorophores[11], [ThT] = 20 μM. λ_{ex} = 340 nm; D) UV absorbance spectra to monitor self-assembly of **CP1** (200 μM) in different conditions.

Therefore, cyclic peptide self-assembly was triggered by controlling the flow of multivalent anions (i.e., SO_4^{2-}) to adjust ionic strength and electrostatic crosslinking[26] and thus adapt the density of the peptide fibrillar network and its spatial position inside the droplet container. Gratifyingly, the corresponding micrographs confirmed the gradual and precise adjustment of the fibres along the droplet container by regulating the flow rates of the electrolyte injection (Figure 4A). An electrolyte shock employing high flow rates of Na_2SO_4 of 150 μL/h led to a strong ionic shielding of the peptide monomers and a crosslinking degree of the protonated microtubular networks. As a consequence, these hydrophilic fibrillar networks concentrated at the core of the droplets (Figure 4A). However, the decrease the electrolyte (SO_4^{-2}) flow rate (e.g., 20 μL/h) allowed the gradual distribution of the supramolecular fibres throughout the water droplet internal volume (Figure 4A right).[5g] Quantification of the fluorescent area in droplet populations confirmed that the higher the electrolyte flow rate, the less the fibrillated fluorescent area per individual droplet (Figure 4B). Comparatively, changes in flow rates using NaOH or $CaCl_2$ did not show such finely tuned trends (Figure S10).

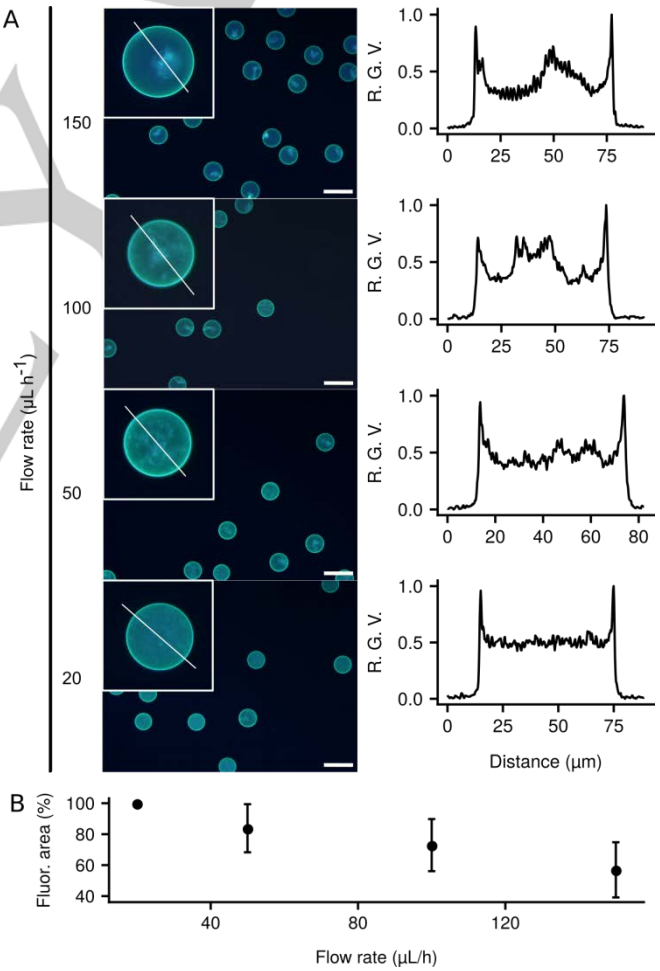

Figure 4. A) Fluorescence micrographs showing network density in the self-assembly of **CP1** in W/O droplets. The peptide (1 mM) was assembled by co-flowing it with Na_2SO_4 5 mM at different flow rates. Flow rates of I_{oil} and I_{CP1} were constant (500 μL h^{-1} and 200 μL h^{-1} respectively). Flow rates of I_T Na_2SO_4 5 mM were varied from 150 to 20 μL/h. Insets denote the traced profile for a representative droplet. Scale bars are 100 μm. B) Percentage of fluorescence area per droplet by image analysis. Average area with standard deviation for the analysis of 20 random droplets. R.G.V. stands for relative gray value.

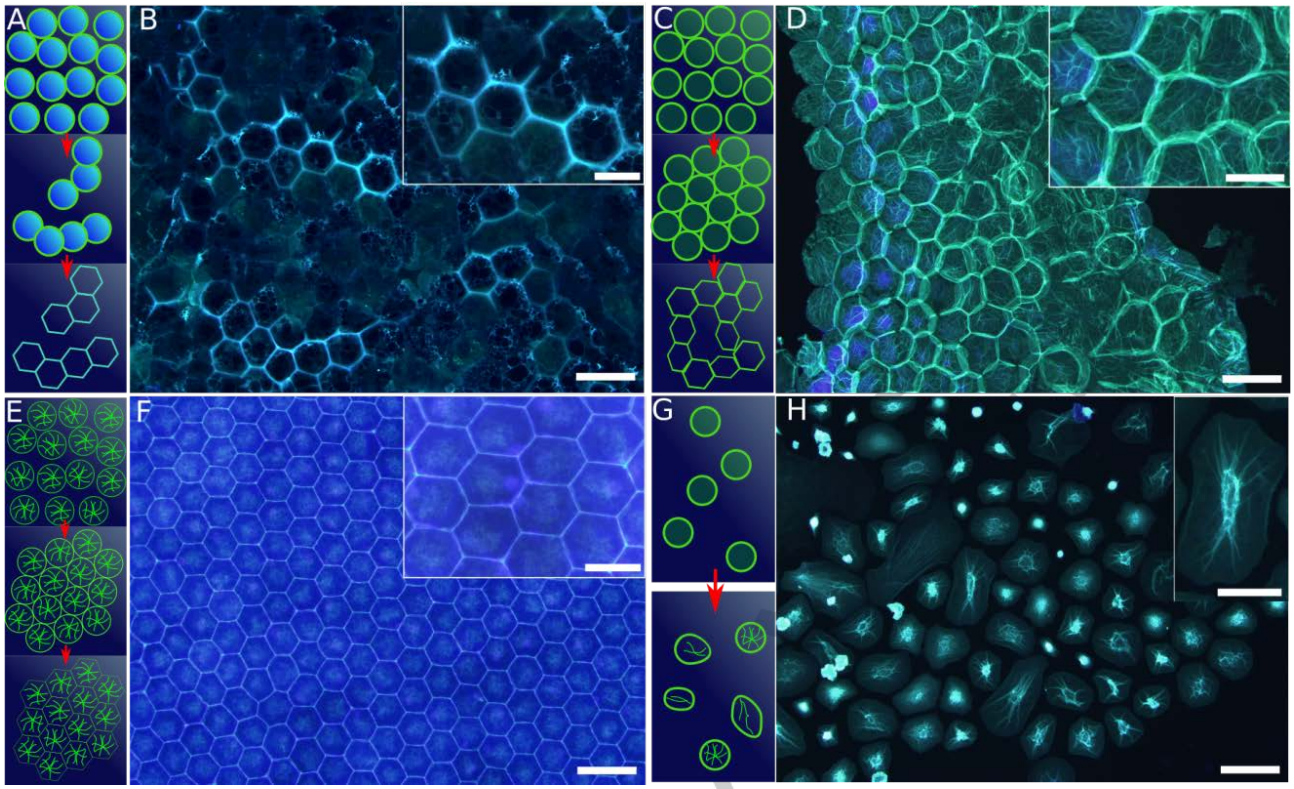

Figure 5. Schematic cartoons depicting the process of Novec oil evaporation and fluorescence microscopy images showing 2D droplet networks after oil evaporation. Red lines in cartoons denote the effect of time lapse. A) and B) Induced droplet assembly in homogenously dispersed **CP1** droplets. C) and D) Induced droplet assembly in cortex-fibrillated droplets (NaOH 3.5 mM); E) and F) Induced droplet assembly in core-fibrillated droplets ($CaCl_2$, 1 M). G) and H) Induced assembly in diluted droplet suspensions over a higher boiling point oil Fluorinert-FC70 (HEPES 50 mM pH 8). A), C), E) and G) are schematic representation of the process, while B), D), F) and H) are epifluorescence images. Scale bars are 100 μm (low magnification) and 50 μm (high magnification).

Spatial control of supramolecular polymerization regulates different communication processes in living systems such as active uptake, multicellular assembly or cell to cell communication.[26] Populations of artificial droplets have also shown adaptive interactions or even "tissue-like" self-organization.[27] Additionally, micro-printing technology has recently allowed the patterning of tissue-like synthetic materials with single droplet resolution.[28] Inspired by functional natural fibrillar networks and the growing importance of droplet micro-patterning, we decided to test if the positional control of the supramolecular polymerization of cyclic peptides could be used to tune assembly of droplet populations.[29] Therefore, the fluorinated oil was carefully evaporated to promote the assembly of water droplets where the polymerization of supramolecular peptide fibres was induced at different positions (Figure 5). Amorphous networks were observed for the assembly of droplets loaded with dispersed cyclic peptides (pH ~ 4), which suggested an uncontrolled aggregation of the droplet suspensions mainly due to disordered surfactant interactions (Figure 5A,B). In contrast, cortex-fibrillated droplets (Figure 2E-H) showed the formation of a roughly assembled network with a green-shifted thick peptide wall with irregular hexagonal and pentagonal patterns. The high curvature topologies and the bathochromic shift of the pyrene emission suggested a strong droplet aggregation triggered by the bundling of the peptide fibres located at the perimeter (Figure 5C,D). However, highly regular hexagonal honeycomb patterns (Figure 5E,F) were formed when the assembly was carried out from droplets suspensions where the fibres were located at the internal core of the droplets (Figure 2I-L). These highly regular networks indicated a more controlled assembly process when the fibres from the droplet core gradually coalesced at the network interface (Figure 5E,F). Finally, anisotropic supramolecular structures, reminiscent of natural fibrillar networks, could also be detected when a droplet emulsion was allowed to dry over a higher boiling point oil (Fluorinert^{TM}-FC70) (See Supporting Information, Figure 5G,H). In this case, the synthetic tubular networks were projected from the droplet core to its periphery and randomly distributed for the smaller spherical droplets. In contrast, anisotropic growth of the supramolecular polymers was confirmed in the direction of the aqueous distribution pattern in elongated droplets (Figure 5H).

Conclusions

In this work, we introduce the spatially-controlled polymerization of supramolecular fibres in water droplets by the microfluidic adjustment of the chemical signals that trigger the self-assembling process. The microfluidic tuning of the chemical nature or the flow rates of the polymerization triggers, allowed the modulation of the tubular network structure and its precisely adjusted spatial position in the different physicochemical environments of a water droplet container (interface *vs* aqueous core). This technology was applied in the generation of well-ordered two-dimensional droplet networks by exploiting the spatially adjusted self-assembly of CP nanotubular bundles. This

work demonstrates the control over the supramolecular polymerization of synthetic fibres in artificial minimal models and suggest the important role of the different chemical environments for the distribution of natural fibrillar networks in simple primitive protocells.

Acknowledgements

This work was partially supported by the Spanish Agencia Estatal de Investigación (AEI) [SAF2017-89890-R, CTQ2016-78423-R], the Xunta de Galicia (ED431G/09, ED431C 2017/25 and 2016-AD031) and the ERDF. A. M.-A. received a MCIF from the EC (GLYCONANOPEP-750248). J. M. holds a Ramón y Cajal (RYC-2013-13784), an ERC-Stg (DYNAP-677786) and a Young Investigator Grant from the HFSP (RGY0066/2017). J. R. G. thanks to the mobility program (PRX17/00147).

Keywords: cyclic peptides • self-assembly • supramolecular chemistry • nanotubes • microfluidics • droplets

References

[1] a) N. Busschaert, C. Caltagirone, W. Van Rossom, P. A. Gale, *Chem. Rev.* **2015**, *115*, 8038–8155; b) F. Trausel, F. Versluis, C. Maity, J. M. Poolman, M. Lovrak, J. H. van Esch, R. Eelkema, *Acc. Chem. Res.* **2016**, *49*, 1440–1447; c) E. Krieg, M. M. C. Bastings, P. Besenius, B. Rybtchinski, *Chem. Rev.* **2016**, *116*, 2414–2477; d) M. J. Webber, R. Langer, *Chem. Soc. Rev.* **2017**, *46*, 6600–6620; e) J. Liu, Y. Lan, Z. Yu, C. S. Y. Tan, R. M. Parker, C. Abell, O. A. Scherman, *Acc. Chem. Res.* **2017,** *50*, 208–217; f) I. Lostalé-Seijo, J. Montenegro, *Nat. Rev. Chem,* **2018**, *2*, 258–277; g) A. M. Garcia, D. Iglesias, E. Parisi, K. E. Styan, L. J. Waddington, C. Deganutti, *Chem*, **2018**, *4*, 1862–1876. h) S. Ulrich, *Acc. Chem. Res.*, **2019**, *52*, 510–519; i) H. Fernández-Caro, I. Lostalé-Seijo, M. Martínez-Calvo, J. Mosquera, J. L. Mascareñas, J. Montenegro, *Chem. Sci.* **2019**, *10*, 8930–8938. j) E. M. Estirado, M. A. Aleman-Garcia, J. Schill, L. Brunsveld, *J. Am. Chem. Soc.*, **2019**, *141*, 18030–18037.

[2] T. Vignaud, L. Blanchoin, M. Théry, *Trends Cell Biol.* **2012**, *22*, 671–682.

[3] A. F. Straight, C. M. Field, *Curr. Biol.* **2000**, *10*, R760–R770.

[4] C. S. Bascom, P. K. Hepler, M. Bezanilla, *Plant Physiol.* **2017**, *176*, 28–40.

[5] a) M. Miyazaki, M. Chiba, H. Eguchi, T. Ohki, S. Ishiwata, *Nat. Cell Biol.* **2015**, *17*, 480–489; b) M. Soares e Silva, J. Alvarado, J. Nguyen, N. Georgoulia, B. M. Mulder, G. H. Koenderink, *Soft Matter* **2011**, *7*, 10631–10641; c) Y. T. Maeda, T. Nakadai, J. Shin, K. Uryu, V. Noireaux, A. Libchaber, *ACS Synth. Biol.* **2011**, *1*, 53–59; d) L. Limozin, M. Brmann, E. Sackmann, *Eur. Phys. J. E* **2003**, *10*, 319–330; e) F.-C. Tsai, G. H. Koenderink, *Soft Matter* **2015**, *11*, 8834–8847; f) Y. Song, T. C. T. Michaels, Q. Ma, Z. Liu, H. Yuan, S. Takayama, T. P. J. Knowles, H. C. Shum, *Nat. Commun.* **2018**, *9*, 2120; g) S. Mellouli, B. Monterroso, H. R. Vutukuri, E. t. Brinke, V. Chokkalingam, G. Rivas, W. T. S. Huck, *Soft Matter* **2013**, *9*, 10493–10500; h) E. te Brinke, J. Groen, A. Herrmann, H. A. Heus, G. Rivas, E. Spruijt, W. T. S. Huck, *Nat. Nanotechnol.* **2018**, *13*, 849–855; i) C. Martino, L. Horsfall, Y. Chen, M. Chanasakulniyom, D. Paterson, A. Brunet, S. Rosser, Y.-J. Yuan, J. M. Cooper, *ChemBioChem* **2012**, *13*, 792–795; j) F. C. Keber, E. Loiseau, T. Sanchez, S. J. DeCamp, L. Giomi, M. J. Bowick, M. C. Marchetti, Z. Dogic, A. R. Bausch, *Science* **2014**, *345*, 1135–1139.

[6] a) J. W. Fredy, A. Méndez-Ardoy, S. Kwangmettatam, D. Bochicchio, B. Matt, M. C. A. Stuart, J. Huskens, N. Katsonis, G. M. Pavan, T. Kudernac, *Proc. Natl. Acad. Sci.* **2017**, *114*, 11850–11855; b) R. Otter, P. Besenius, *Org. Biomol. Chem.* **2019**, *17*, 6719–6734; c) D. Bochicchio, S. Kwangmettatam, T. Kudernac, G. M. Pavan, *ACS Nano* **2019**, *13*, 849–855; d)J. Leira-Iglesias, A. Tassoni, T. Adachi, M. Stich, T. M. Hermans, *Nat. Nanotechnol.* **2018**, 1021–1027.

[7] R. Booth, I. Insua, G. Bhak, J. Montenegro, *Org. Biomol. Chem.* **2019**, *17*, 1984–1991.

[8] R. J.R. W. Peters, M. Marguet, S. Marais, M. W. Fraaije, J. C. M. van Hest, S. Lecommandoux, *Angew. Chem. Int. Ed.* **2013**, *53*, 146–150.

[9] R. Krishna Kumar, X. Yu, A. J. Patil, M. Li, S. Mann, *Angew. Chem. Int. Ed.* **2011**, *50*, 9343–9347.

[10] D. S. Ferreira, R. L. Reis, H. S. Azevedo, *Soft Matter* **2013**, *9*, 9237–9248.

[11] A. Méndez-Ardoy, J. R. Granja, J. Montenegro, *Nanoscale Horiz.* **2018**, *3*, 391–396.

[12] a) M. Weiss, J. Frohnmayer, L. Benk, B. Haller, J.-W. Janiesch, T. Heitkamp, M. Börsch, R. Lira, R. Dimova, R. Lipowsky, E. Bodenschatz, J.-C. Baret, T. Vidakovic-Koch, K. Sundmacher, I. Platzman, J. Spatz, *Nat. Mater.* **2017**, *17*, 89–96; b) N.-N. Deng, M. Yelleswarapu, L. Zheng, W. T. S. Huck, *J. Am. Chem. Soc.* **2016**, *139*, 587–590; c) N.-N. Deng, M. A. Vibhute, L. Zheng, H. Zhao, M. Yelleswarapu, W. T. S. Huck, *J. Am. Chem. Soc.* **2018**, *140*, 7399–7402.

[13] R. K. Shah, H. C. Shum, A. C. Rowat, D. Lee, J. J. Agresti, A. S. Utada, L.-Y. Chu, J.-W. Kim, A. Fernandez-Nieves, C. J. Martinez, D. A. Weitz, *Mater. Today* **2008**, *11*, 18–27.

[14] A. Sorrenti, R. Rodriguez-Trujillo, D. B. Amabilino, J. Puigmarti-Luis, *J. Am. Chem. Soc.* **2016**, *138*, 6920–6923.

[15] H. Shaikh, J. Y. Rho, L. J. Macdougall, P. Gurnani, A. M. Lunn, J. Yang, S. Huband, E. D. H. Mansfield, R. Peltier, S. Perrier, *Chem. Eur. J.* **2018**, 19066–19074.

[16] a) M. R. Ghadiri, J. R. Granja, R. A. Milligan, D. E. McRee, N. Khazanovich, *Nature* **1993**, *366*, 324–327; b) J. Montenegro, M. R. Ghadiri, J. Granja, *Acc. Chem. Res*., **2013**, *46*, 2955–2965; c) N. Rodríguez-Vázquez, M. Amorín, J. R. Granja, *Org. Biomol. Chem.* **2017**, *15*, 4490–4505; d) I. Insua, J. Montenegro, *J. Am. Chem. Soc.* DOI:10.1021/jacs.9b10582.

[17] a) J. Y. Rho, J. C. Brendel, L. R. MacFarlane, E. D. H. Mansfield, R. Peltier, S. Rogers, M. Hartlieb, S. Perrier, *Adv. Funct. Mater.* **2017**, *28*, 1704569; b) M. Cuerva, R. García-Fandiño, C. Vázquez-Vázquez, M. A. López-Quintela, J. Montenegro, J. R. Granja, *ACS Nano* **2015**, *9*, 10834–10843; c) J. Montenegro, C. Vázquez-Vázquez, A. Kalinin, K. E. Geckeler, J. R. Granja, *J. Am. Chem. Soc.* **2014**, *136*, 2484–2491.

[18] A. Fuertes, M. Juanes, J. R. Granja, J. Montenegro, *Chem. Commun.* **2017**, *53*, 7861–7871.

[19] G. M. Kontogeorgis, S. Kiil, *Introduction to Applied Colloid and Surface Chemistry*, John Wiley & Sons, Ltd, **2016**.

[20] a) D. A. Walker, B. Kowalczyk, M. O. de la Cruz, B. A. Grzybowski, *Nanoscale* **2011**, *3*, 1316–1344; b) J. Stendahl, M. Rao, M. Guler, S. Stupp, *Adv. Funct. Mater.* **2006**, *16*, 499–508.

[21] Assembly kinetics and theoretical calculations suggest that although self-assembly might be initiated before droplets formation, equilibration takes place in the droplet (Section S3 in the Supplementary Information).

[22] C. Holtze, A. C. Rowat, J. J. Agresti, J. B. Hutchison, F. E. Angil, C. H. J. Schmitz, S. Kster, H. Duan, K. J. Humphry, R. A. Scanga, J. S. Johnson, D. Pisignano, D. A. Weitz, *Lab. Chip* **2008**, *8*, 1632–1639.

[23] a) J. Zhang, R. J. Coulston, S. T. Jones, J. Geng, O. A. Scherman, C. Abell, *Science* **2012**, *335*, 690–694; b) J. Zhang, J. Liu, Z. Yu, S. Chen, O. A. Scherman, C. Abell, *Adv. Funct. Mater.* **2018**, *28*, 1800550.

[24] C. Kurokawa, K. Fujiwara, M. Morita, I. Kawamata, Y. Kawagishi, A. Sakai, Y. Murayama, S.-i. M. Nomura, S. Murata, M. Takinoue, M. Yanagisawa, *Proc. Natl. Acad. Sci.* **2017**, *114*, 7228–7233.

[25] M. Biancalana, S. Koide, *Biochim. Biophys. Acta Proteins Proteomics* **2010**, *1804*, 1405–1412.

[26] M. Baker, *Nature*, **2017**, *549*, 322–324.

[27] a) H. Niederholtmeyer, C. Chaggan, N. K. Devaraj, *Nat. Commun.* **2018**, *9*, 5027; b) P. Gruner, B. Riechers, B. Semin, J. Lim, A. Johnston, K. Short, J.-C. Baret, *Nat. Commun.* **2016**, *7*, 10392; c) K. M. Chang, M. R. R. de Planque, K.-P. Zauner, *Sci. Rep.* **2018**, *8*, 12656.

[28] G. Villar, A. D. Graham, H. Bayley, *Science* **2013**, *340*, 48–52.

[29] P. Zhu, T. Kong, C. Zhou, L. Lei, L. Wang, *Small Methods* **2018**, *2*, 1800017.

Entry for the Table of Contents (Please choose one layout)

Layout 1:

RESEARCH ARTICLE

Spatially regulated assembly of synthetic supramolecular fibers is controlled in a microfluidic device. Modulation of chemical triggers such as pH or ionic strength allowed the spatial organization of supramolecular fibers confined in water droplets. 2D suprastructures can be assembled by controlling the organization of droplet and fibrillar assembly.

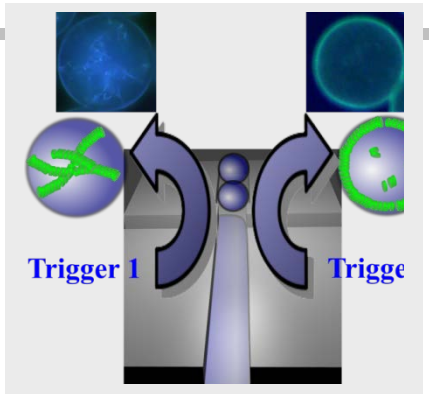

Alejandro Méndez-Ardoy, Alfonso Bayón-Fernández, Ziyi Yu, Chris Abell, Juan R. Granja, Javier Montenegro**

Page No. – Page No.

Spatially Controlled Supramolecular Polymerization of Peptide Nanotubes by Microfluidics

Layout 2:

RESEARCH ARTICLE

((Insert TOC Graphic here. **Note**: Please provide a legible image, 11×2.5 cm (w×h), min. font size 6-7 pt.))

*Author(s), Corresponding Author(s)**

Page No. – Page No.

Title

Text for Table of Contents, 450 characters with spaces.